




Synthesis of zeolites from volcanic ash (Tajogaite, Spain) for the remediation of waters contaminated by fluoride

Iker Martínez-del-Pozo¹ · José María Esbri¹ · Luz García-Lorenzo¹ · Sol López-Andrés¹ 

Received: 25 September 2023 / Accepted: 15 December 2023 / Published online: 29 December 2023
© The Author(s), under exclusive licence to Springer-Verlag GmbH Germany, part of Springer Nature 2023

Abstract

In the eruptive event of Tajogaite (2021) in La Palma, Canary Islands, large quantities of volcanic ash were accumulated, affecting the local environment and urban areas. In this study, volcanic ash sampled from urban areas (catalogued as municipal waste (20 03 03) by the European Wastes Catalogue) were converted into zeolites by hydrothermal synthesis at 100 °C with previous alkaline fusion at 550 °C with distilled water. During this process, new phases of zeolite principally type X and sodalite have been identified by XRD at 2 h of incubation. These zeolites, with the course of incubation time, present competitive processes where the transformation into sodalite develops after 24 h as the predominant phase. The synthesized zeolitic material presents a high concentration as impurities in Fe₂O₃ (13.70 wt%), Na₂O (12.70 wt%), CaO (11.65 wt%), and TiO₂ (3.89 wt%) coming from the volcanic ash and NaOH introduced in the synthesis methodology. These impurities impart different physicochemical capabilities to the zeolitic material. The application of zeolites obtained in a preliminary fluoride adsorption experiment with volcanic leachate water rich in fluoride has been tested in a novel way. Removal efficiencies of 41.4% at acidic pH (5.77) have been obtained with 2 g L⁻¹ adsorbent zeolitic material doses. A value-added material is obtained and applied in a preliminary way to solve a problem generated by the volcanic ash itself, allowing the End of Waste status and meeting different objectives of the sustainable development goals of the UN Agenda 2030.

Keywords Volcanic ash · Zeolite · Hydrothermal synthesis · Fluoride remediation · Adsorption · Impurities · Mineralization

Introduction

La Palma is the most active volcanic island of the Canary Islands, located west of the Western Sahara and Morocco coasts. The last 7 of the 14 historical eruptive events of the archipelago have originated on this island, the last one being in 2021 (Longpré and Felpeto 2021; Carracedo et al. 2022). This event is characterized by multiple eruptive styles with strombolian explosions, phreatomagmatic pulses, and effusive activity with a duration of 85 days (from September 19 to December 13, 2021), with the extrusion of lava fountains and with an emission of 45×10^6 m³ of particulate material into the atmosphere (Bonadonna et al. 2022; Carracedo

et al. 2022). During the extrusion of this material, there were interactions in the volcanic plume with different volcanic gases such as H₂O, CO₂, SO₂, H₂, H₂S, CO, HCl, and HF, generating volcanic ashes with a composition characterized by the presence of crystallized minerals, glass and rocks, in addition to sulfate, chloride, and fluorine salts precipitated on the surfaces of the volcanic ashes (Le Maitre 2002; Delmelle et al. 2007; Ruggieri et al. 2010, 2012; Barone et al. 2016). Finer volcanic ash can be transported hundreds or thousands of kilometers from emission points. This transport occurs as aerosol particles and finer volcanic glass. In the Tajogaite eruption, these materials were detected in Eastern Europe and Central America, a phenomenon favored by action of winds and atmospheric currents (Carracedo et al. 2022).

Volcanic ash can generate multiple impacts and affections. For example, in the atmosphere, it can disrupt aviation (Jenkins et al. 2015; Lechner et al. 2018) and in the environmental compartments, introducing nutrients such as Fe, Mn, Ca, and P but also incorporating potentially toxic elements (PTEs) such as As, Cu, F, Mo, Ni, Pb, and Zn by inserting

Responsible Editor: George Z. Kyzas

✉ Sol López-Andrés
antares@ucm.es

¹ Departamento de Mineralogía y Petrología, Facultad de Ciencias Geológicas, Universidad Complutense de Madrid, Calle José Antonio Nováis, 12, 28040 Madrid, Spain

and dispersing through environmental compartments (Jones and Gislason 2008; Fernández-Turiel et al. 2012; Ermolin et al. 2018). When this volcanic material accumulates in urban areas, it can cause structural damage to civil works and develop building collapses (Jenkins et al. 2015). Ash falls and washing activities can be resuspended, causing human health affection by entering the respiratory tract and causing asthma, bronchitis, eyes and skin irritation, among others (Horwell and Baxter 2006; Barsotti et al. 2010; Jenkins et al. 2015), specifically in the 2 km close to the active eruptive focus (Ruggieri et al. 2023). A short-, medium- and long-term epidemiological study related to this condition has been conducted by Ruano-Ravina et al. (2023).

When volcanic ash accumulated in urban areas, it is classified by European Wastes Catalogue as municipal waste (code 20 03 03) (Environmental Protection Agency 2010). The volume of this material on the La Palma Island generates an added problem in the management of this waste since they must be transported and deposited in large landfills. To solve this problem, this waste can be recycled as raw material and revert the status to “End of Waste” by Directive 2008/98/EC of European Parliament (European Council 2008). These wastes can be used in different ways, presenting multiple applications due to the chemical composition and their structural properties that can be used for example in construction materials (Kupwade-Patil et al. 2018), in the production of geopolymers (Muñoz Pérez Sócrates et al. 2022), recyclable catalytic materials (Muñoz et al. 2019), alkali-activated binders (Mañosa et al. 2023), etc. Another interesting application of volcanic ashes is the production of value-added materials by synthesis processes to form zeolites (Arroyo et al. 2021; Belviso et al. 2021; Monzón et al. 2021).

Zeolites are microporous aluminosilicate minerals composed by (Si,Al)O₄ tetrahedra forming ring structures (Cejka et al. 2011). In zeolite structures, Si⁴⁺ is replaced by Al³⁺, resulting in a positive charge deficiency that is balanced by the presence of Na⁺, K⁺, Ca²⁺, and Mg²⁺ generating the electroneutrality of the structures (Cejka et al. 2011; Jha and Singh 2011). In zeolite, isomorphism might be possible by substituting the framework element (Si and Al) to include transition metals (Ti, Fe, Cu, Mn, W, etc.) (Zhang et al. 2022). The general formula is $M_{2/n}O \cdot Al_2O_3 \cdot xSiO_2 \cdot yH_2O$, where *M* is any alkali metal (Na, Ca, K, Ba or Sr); *n* is the valence of the cation; *x* is a variable number between 2 and 10, and *y* is a number between 2 and 7 (Cejka et al. 2011). The types of zeolites formed depend on temperature, pressure, pH, synthesis activation, and SiO₂/Al₂O₃ content of the starting feedstock (Jha and Singh 2011). Synthetic zeolites can be obtained by chemical processes following multiple methodologies (conventional hydrothermal synthesis, microwave-assisted hydrothermal method, fusion and hydrothermal method, and molten salt synthesis (Jha and Singh

2011)), taking as raw material wastes with high aluminum content. Fly ash from industrial waste is commonly used to synthesize zeolites (Belviso et al. 2010, 2012, 2019; He et al. 2016; Sánchez-Hernández et al. 2016, 2017, 2018a; López Delgado et al. 2017; Han et al. 2019; López-Delgado et al. 2020; Zhou et al. 2023). In more exceptional and innovative cases, volcanic natural materials have been used for these purposes with tuff with scoriaceous clasts and bombs from Vico volcano (Italy) (Novembre et al. 2004), volcanic tephra particles from Changbai Mountains (China) (Wang et al. 2015), scoria from Jeju Island (Korea) (Lee et al. 2018), volcanic ash extracted from volcanic tuffs from Mt. Eburu volcano (Kenya) (Otieno et al. 2023), and, more exceptionally, volcanic ash has recently been used to synthesize zeolite from Chaitén volcano (Chile) (Sanhueza-Núñez and Bennun-Torres 2015), Colima volcano (Mexico) (Luévano-Hipólito et al. 2021), Mt. Etna (Italy) (Belviso et al. 2021; Gagliano et al. 2022), Ubinas volcano (Peru) (Almirón et al. 2022), and Puyehue-Cordón Caulle (Argentina) (Monzón et al. 2021; Muñoz et al. 2023).

Physical properties, such as pore interconnection and chemistry properties, such as ion exchange capacity, catalysis, molecular filter, and adsorption capacity give zeolites multiple applications in different sectors (Jha and Singh 2011). The use of zeolites to combat some environmental challenges promotes the Sustainable Development Objectives of the United Nations 2030 Agenda (Naciones Unidas/CEPAL 2019). Decontamination of water with zeolites can reduce diseases caused by water and soil pollutants (SDG 3 “Good Health and Well-Being” target 3.9). This treatment can improve the quality of water resources (SDG 6 “Clean Water and Sanitation” target 6.3) achieving environmentally sound waste management and efficient use of natural resources (SDG 12 “Responsible Consumption and Production” target 12.2 and 12.4). In the environmental sector, zeolites can remove radioisotopes such as ¹³⁷Cs and ⁹⁰Sr from radioactive wastewater to remove cationic PTEs such as As⁵⁺, Pb²⁺, Cd²⁺, Cu²⁺, Zn²⁺, Hg, and NH⁴⁺ from wastewater, as well as reduce the salinity, sodicity of different waters, and capture of CO₂ (He et al. 2016; Sánchez-Hernández et al. 2018b; Han et al. 2019; Ge et al. 2020; Belviso et al. 2021; Wen et al. 2021; Gagliano et al. 2022; Hamoud et al. 2023; Zhou et al. 2023). Another application in the environmental area is the adsorption of fluoride in contaminated water, as occurs locally on the island of La Palma after the eruption by the secondary minerals condensed on the surface of the particles when they dissolve in contact with water (Amonte et al. 2022; Rodríguez et al. 2022; Ruggieri et al. 2023; Sánchez-España et al. 2023). This could increase the concentration of fluoride above the quality standards set at 1.5 mg/L (World Health Organization 2022), which could generate multiple pathologies, especially in children and pregnant women (Ayoob and Gupta 2006; Zuo et al. 2018).

In the last decade, the use of zeolite for defluoridation of waters with high fluoride concentration from zeolite synthesized by fly ash has received much attention due to the few existing technologies for their removal (Habuda-Stanić et al. 2014; Kumar et al. 2019). Zeolites are good at adsorbing cations; however, they are not as good at adsorbing anions, but modification with different elements such as Fe^{3+} , Al^{3+} , Ca^{2+} , and Na^+ can change their physicochemical properties by developing increased capacity to adsorb anions such as fluoride as seen in zeolites modified from fly ash and natural zeolites primary material and different additives (Onyango et al. 2004; Rahmani et al. 2010; Sun et al. 2011; Zhang et al. 2011; Gómez-Hortigüela et al. 2013; Teutli-Sequeira et al. 2014; Ranasinghe et al. 2022). The use of zeolites synthesized from volcanic ash for fluoride adsorption has not been found in recent literature. This type of defluoridation with materials transformed from VA can solve a double problem at the local level, such as the disposal of the residue and the decontamination of the fluoride generated by the VA itself.

The aim of this study is the synthesis of zeolites to reverse the waste condition of volcanic ashes deposited in urban areas and the evaluation of its use in the remediation of waters contaminated by fluorides. To accomplish this main objective, a complete characterization of the waste (volcanic ash) will be carried out, followed by a hydrothermal synthesis of zeolites with a high temperature pre-fusion method. The mineralogical evolution will be investigated for different incubation times (up to 120 h) and the crystallization mechanism at those times will be studied. Given the fluoride contamination generated by the eruption, the use of the zeolitic material as a by-product in the defluorination of leached water with volcanic ash will be evaluated during preliminary adsorption experiments at different pH and dosages.

Materials and methods

Volcanic ash sampling

Volcanic ash (VA) from Tajogaite (2021) eruption was used as raw material. The VA was sampled at 4175 m north of the emission centers, specifically in El Paso, (Canary Islands, Spain) (X 219.170 and Y 3.172.541, WGS84) on 27/11/21. The sample was collected with a plastic shovel from an ash accumulation located in the interior courtyard. The interior courtyard was cleaned daily by the cleaning services, consequently the sample has not been altered by weathering or anthropogenic contamination. The material was placed in polypropylene bags for transport to the laboratory, where it was homogenized and quartered into 8 fractions of 586 g. One of these fractions was used for the present study. This volcanic ash material was destined for landfill disposal, as it

is classified as municipal waste from various miscellaneous cleaning under the mixed waste section (20 03 03) according to the European Waste Catalogue (Environmental Protection Agency 2010). The use of this material, as with all waste, requires a complete prior characterization.

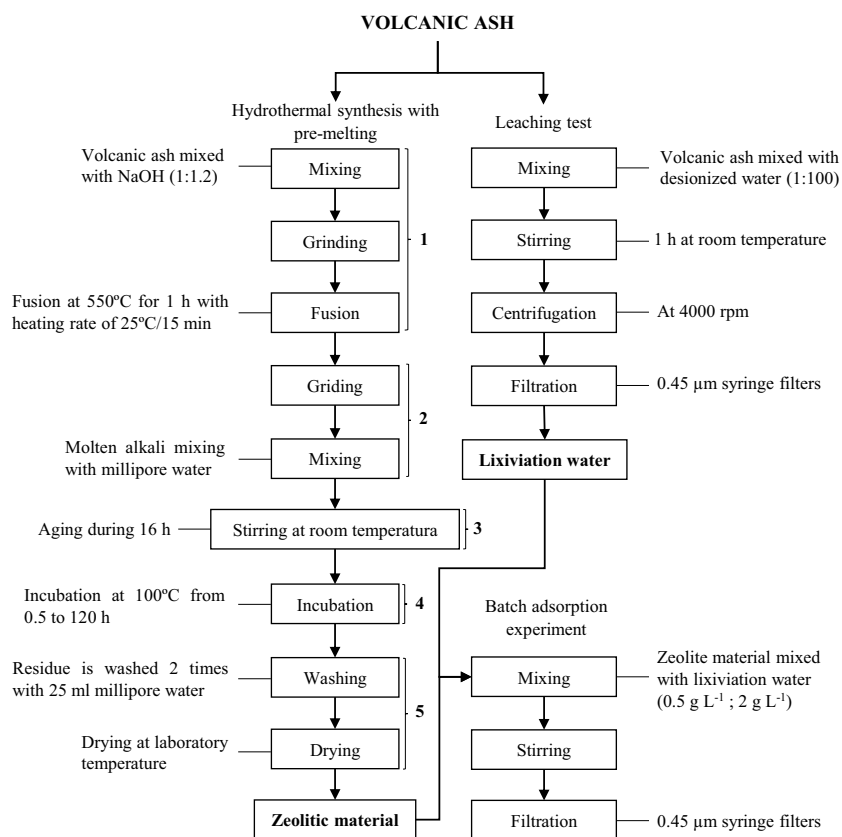
Zeolite synthesis experiments

In this studio, the zeolite synthesis process was performed by various methodologies (Chang and Shih 1998; Belviso et al. 2010, 2012, 2021), summarized in Fig. 1, essentially by hydrothermal synthesis with pre-melting developed in five steps: Step 1, a 1:1.2 weight ratio of volcanic ash and solid NaOH was mixed, ground, and melted at 550 °C for 1 h with heating ramp of 25 °C every 15 min. Step 2, 8.8 g of alkaline fusion product was mixed with 43 mL of ultrapure water. Step 3, the dispersion mixture from step 2 was stirred at laboratory room temperature continuously for 16 h. Step 4, the mixture was placed in eight pyrex beakers covered with watch glasses. This mixture was heated at 100 °C for 0.5, 1, 2, 4, 8, 24, 96, and 120 h. Step 5, the solution was separated from the solid by filtration, measuring the volume of remaining water. The solid was washed twice with 25 mL of ultrapure water and dried at laboratory room temperature.

Characterization of VA and synthetic samples

A complete granulometric, chemical, mineralogical, and morphological characterization of initial volcanic ash and the different synthetic products has been carried out. The granulometric characterization was determined by phi scale and laser diffraction granulometry with the Honeywell Microtrac X100 equipment. Mineralogical composition was determined by X-ray diffraction (XRD) using the polycrystalline powder methodology by Bruker D8 Advance diffractometer equipped with Cu $K\alpha$ radiation and graphite monochromator. The XRD patterns were collected between 10 and 60° angular range of 2θ , step size of 0.02°, and scanning step time of 1 s. Samples were milled and sieved at 53 μm . The crystalline phases were identified by EVA DIFFRACplus 13.0 with comparisons with the PDF2 (Powder Diffraction File) database of the ICDD (International Center for Diffraction Data) (Blanton et al. 1995). The Xpowder analytical software version 12 was used for the semi-quantitative determination of the amorphous and crystalline phase (Martin 2004). The diffractograms obtained have been smoothed with the program EVA DIFFRACplus 13.0. The chemical composition of the volcanic ash (VA) was determined by energy dispersive X-ray fluorescence (EDXRF) with the Bruker S2 Ranger equipment for the analysis of the major and minor elements using the EQUA Oxides calibration method. A sub-sample of 9.2 and 0.8 g of wax was used to prepare a pressed pill. The trace elements were determined

Fig. 1 Flow chart of hydrothermal synthesis with prior melting process (modified from Jha and Singh 2011), leachate test and batch adsorption experiments



by ICP-OES with the SPECTRO Arcos equipment. The chemical composition of the zeolite samples was determined by EDXRF with sub-samples of 4.6 and 0.4 g of wax. Morphological analyses were performed by scanning electron microscopy (SEM) with a JEOL JSM 820 equipment, and the micro-chemical analyses were achieved by X-ray dispersion spectrometer (XDS) with Oxford Link with 20 kv accelerating voltage. The sub-sample was deposited on gold metalized graphite tape. The pH and electrical conductivity (EC) of the solutions were measured with a pH-Meter Crison Basic 20 and a Crison Micro CM 2200 conductometer. All the analyses were performed at the Geological Techniques Unit (Center for Research Assistance in Earth Sciences and Archeometry) of the Complutense University of Madrid (UCM).

Volcanic ash leaching test and preliminary fluoride adsorption experiments

The volcanic ash leaching tests have been carried out following the IVHHN procedure described by Stewart et al. (2020). The leaching experiments have been carried out following the protocol of IVHHN and Stewart et al. (2020) with the ratio of 1:100 solid/liquid. The protocol recommends carrying out two types of tests, 1:20 and 1:100. However, our objective was to obtain a leachate with a high concentration

of F in the aqueous medium, therefore analyzing the study by Ruggieri et al. (2023), where the same protocol follows indicates that the 1:20 ratio can become supersaturated. That is why, the relationship has been chosen where those crystals adsorbed to the surface of the CV can be leached in greater quantities. Therefore, a 1:100 weight ratio of volcanic ash and millipore water was mixed (6 g of volcanic ash was mixed with 600 mL of ultrapure water). The mixture was stirred for 1 h at room temperature on a magnetic stirrer at 200 rpm. After the stirring process, the pH and electrical conductivity were measured. The leachates were then centrifuged at 4000 rpm for 10 min with a P-Selecta Cenicon II centrifuge and filtered with 0.45-µm Branchia CA-syringe filters. Portion of this leachate (CL-1) was reserved for analysis of its initial total fluoride concentration. The rest of the leachate was used to perform the batch adsorption experiments. The defluoridation experiments were performed using a fischerbrand blender at 80 rpm. The experiments were performed at different pH levels (10.8 and 5.7), different synthetic zeolitic materials (SZ-3, SZ-4, and SZ-6). The alkaline pH mixture was prepared with SZ-3, SZ-4, and SZ-6 synthetic zeolitic materials, while the acidic was prepared only with SZ-4 synthetic zeolitic material. The acidic pH mixture was adjusted with HCl 0.1 M obtaining a final pH of 5.74 and 5.77. These four experiments were mixed with different adsorbent doses: 0.5 g and 2 g L⁻¹ of synthesized

zeolitic material on 50 mL of leached water. A ContrAA700 high-resolution continuum source atomic absorption spectrometer Analytik Jena in ICTAN (Instituto de Ciencia y Tecnología de los Alimentos y Nutrición, Spain) was used for total fluoride analysis of all samples. The removal efficiency ($E\%$) were calculated using Eq. (1):

$$E(\%) = \frac{(C_o - C_{eq}) \times 100}{C_o} \quad (1)$$

where E represents fluoride removal efficiency (%); C_o initial fluoride concentration (mg L^{-1}); and C_{eq} equilibrium concentration (mg L^{-1}).

Results and discussion

Raw material — volcanic ash characterization

For the correct use of a waste, such as volcanic ash deposited in the urban areas of La Palma, the first step is its complete characterization.

The particle size distribution of volcanic ash can be classified according to Le Maitre (2002) as coarse ash (63 to 1000 μm) with 89%, followed by fine ash grain (< 63 μm) with 10% and lapilli (> 1000 μm) with 1% (Fig. 2). The XRD profile (Fig. 3) of the initial volcanic ash sample is characterized by the presence of detectable amorphous phase with a broad band from 17 to 36° 2θ and a crystalline phase with different mineral identifications: plagioclase (labradorite PDF 83–1417), clinopyroxene (diopside PDF 72–1497), olivine (PDF 72–2461), amphibole (kaersutite PDF 44–1450), titanomagnetite (PDF 75–1376), hematites (PDF 72–0469), and ilmenite (PDF 75–1203). Mineral composition follows the line described for tephtras by Carracedo et al. (2022) and Sánchez-España et al. (2023). The semi-quantification or estimation of the amorphous phase and crystalline phases is shown in Table 1.

The chemical data of the major, minor, and trace elements in the VA sample are shown in Table 2. The data show a high concentration of Fe_2O_3 (15.1 wt%), CaO (12.03 wt%), and TiO_2 (4.3 wt%). The concentrations of PTEs were low. The sample can be classified by TAS diagram (Le Maitre 2002) as a tephrite-basanite material. These mineralogical and chemical compositions agree

Fig. 2 Granulometric distribution of percentage passing of particle size distribution of CS sample

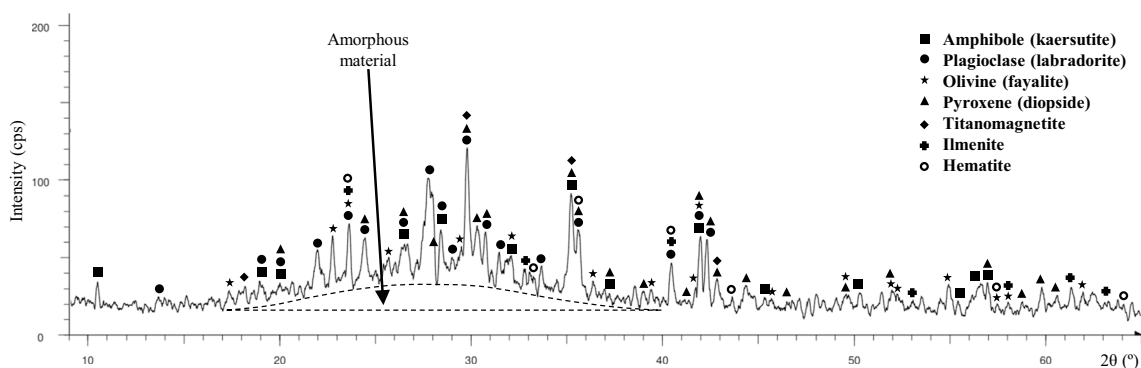
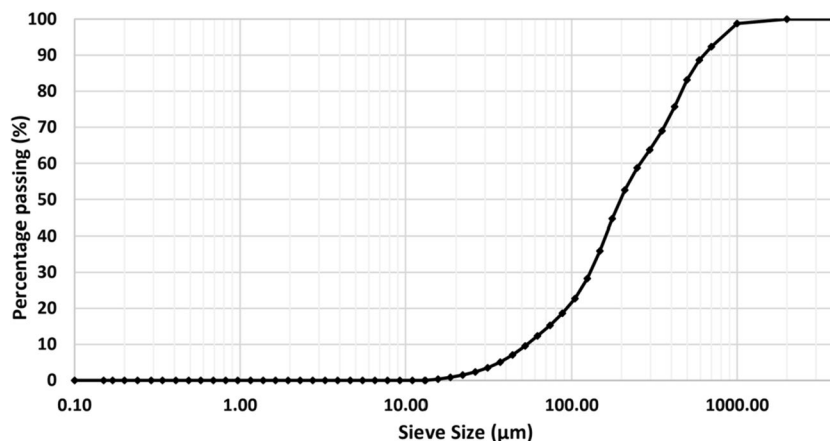


Fig. 3 X-ray diffraction patterns of CS sample

Table 1 Proportions of amorphous and crystalline phases and main mineral phases of VA sample

Volcanic ash	wt%
Amorphous phase	24.30
Crystalline phase	75.70
Plagioclase	36.60
Pyroxene	15.50
Olivine	8.00
Amphibol	6.10
Titanomagnetite	4.00
Hematite	3.50
Ilmenite	2.00

with data from the analysis of pyroclastic material from the same eruption (Carracedo et al. 2022). The $\text{SiO}_2/\text{Al}_2\text{O}_3$ ratio is 2.74.

The morphological observations and microanalyses of VA by SEM allow us to determine the nanometric and micrometric dimensions of the integrating particles and the existence of phenocrysts and vitreous material. The phenocrysts presented an angular morphology of 150–800 μm size, where their mineral lamination can be observed (Fig. 4A). An example of microanalysis of these phases is shown in Fig. 4. Regarding the amorphous material, they presented elongated particles with fluid texture of 60–350 μm in size (Fig. 4B). Examples of volcanic amorphous microanalysis are shown in Fig. 4. Also, vesicular texture of 80–300 μm size can be observed (Fig. 4A and C). The chemical composition of phenocrysts and glassy/amorphous volcanic material were the main source of Si, Al, and O of the structural base of the future zeolites. The remarkable presence of Ca observed in both EDXRF and EDXs will condition the zeolite species synthesized. In addition, Fe and Ti contents can be introduced in the

zeolitic structures as impurities together with different trace elements.

An abundance of micrometric secondary crystals with pseudolaminar and cubic habit in some cases were observed on all particle surfaces (Fig. 4B, C, and D). Chemical composition of these crystals shows a content in Al, Si, Ca, Na, O, and high content of F, from 43.98 to 51.41 wt%. These crystalline aggregates are interpreted as high soluble salts, CaF_2 and AlF_3 , according to Sánchez-España et al. (2023). These fluorinated secondary minerals present a morphology and chemical composition, without presence of dissolution phenomena, possibly due to the rapidity of ash collection, within a few hours of deposition. However, Sánchez-España et al. (2023) observed a greater morphological variety, and Ruggieri et al. (2023) have not been able to observe these soluble fluorine minerals in the SEM.

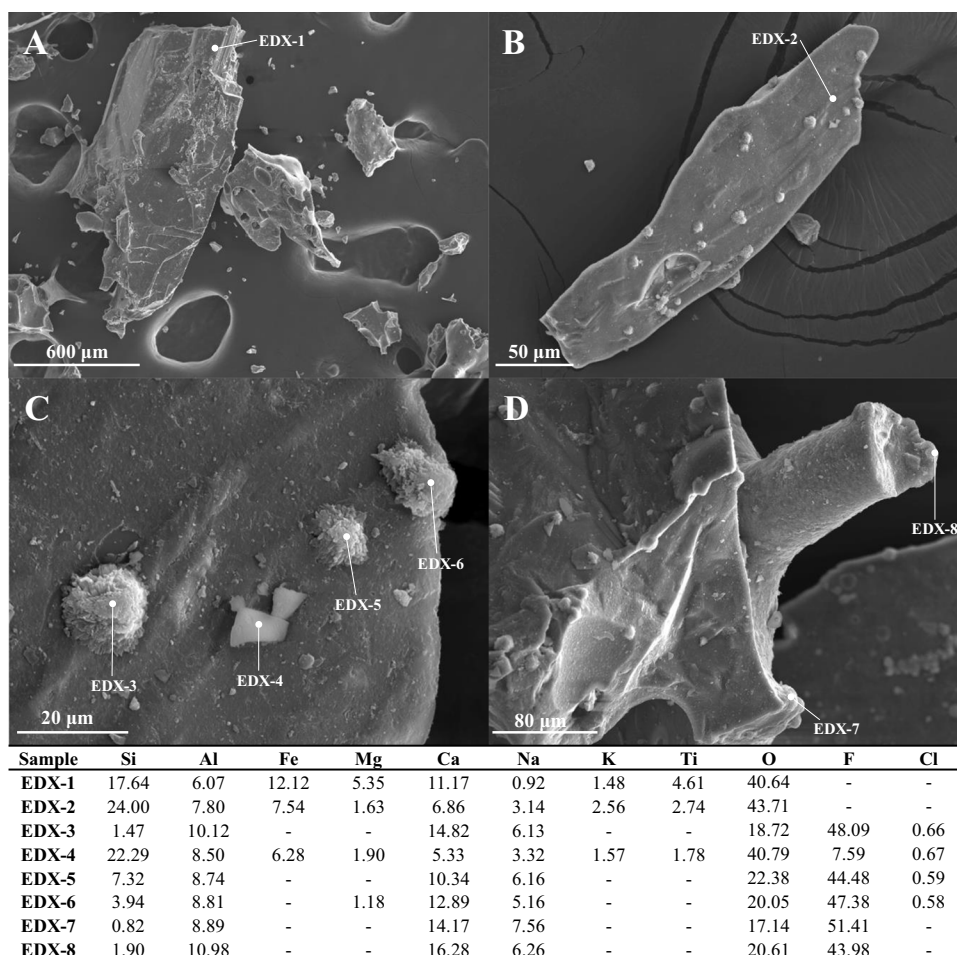
Zeolite synthesis processes

XRD patterns of the synthesis product obtained after the hydrothermal incubation process at 100 °C during 0.5 to 120 h are shown in Fig. 5. The alkaline activation, developed in step 1 (Fig. 1), generates the destruction by dissolution of the main minerals of the initial volcanic ash to form new phases (SZ-0). New crystalline phases are identified in the product obtained from the alkaline fusion from volcanic ash and NaOH: thermonatrite (PDF 08–0448, $\text{Na}_2\text{CO}_3 \cdot \text{H}_2\text{O}$), natrite (PDF 37–0461, Na_2CO_3), hydrated sodium aluminum oxyhydroxide (PDF 48–0289, $\text{Na}_2(\text{Al}_2\text{O}_3(\text{OH})_2) \cdot 1.5\text{H}_2\text{O}$), and amorphous aluminosilicate material. The mixture of molten alkaline with ultrapure water caused an increase in pH from 7.82 in the initial water to 13.23 in the new solution in contact with alkaline fusion material, creating a favorable environment for the dissolution of the sodium phases formed. Aqueous medium was supersaturated, increasing the

Table 2 Multielemental composition of VA sample and synthesized material after 2 h of incubation. Major elements and trace elements were determined by EDXRF (expressed in wt%)

VA sample				Synthesized material (SZ-3 with 2-h incubation)			
Major and minor elements		Trace elements		Major and minor elements		Trace elements	
Oxides	(wt%)	Oxides	(wt%)	Oxides	(wt%)	Oxides	(wt%)
SiO_2	41.19	SrO	0.20	SiO_2	37.26	MnO	0.07
Fe_2O_3	15.05	MnO	0.08	Al_2O_3	15.58	ZrO_2	0.07
Al_2O_3	14.91	ZrO_2	0.08	Fe_2O_3	13.70	Cr_2O_3	0.03
CaO	12.03	V_2O_5	0.07	Na_2O	12.70	ZnO	0.03
MgO	4.40	CuO	0.01	CaO	11.65		
TiO_2	4.26	SnO_2	0.01	MgO	4.00		
Na_2O	3.50			TiO_2	3.89		
K_2O	2.44			K_2O	0.84		
P_2O_5	0.99			SrO	0.18		
Cl	0.38						
SO_3	0.36						

Fig. 4 Secondary electrons (SE) SEM images of CS sample: **A** image of ash particle with blocky and vesicular texture at 100×; **B** image of fluidal ash particle with multiple secondary crystals on the surface at 450×; **C** image from **B** surface particle at 3000×; **D** image of vesicular texture with secondary crystals at 700×. Spot chemical microanalysis (wt%)

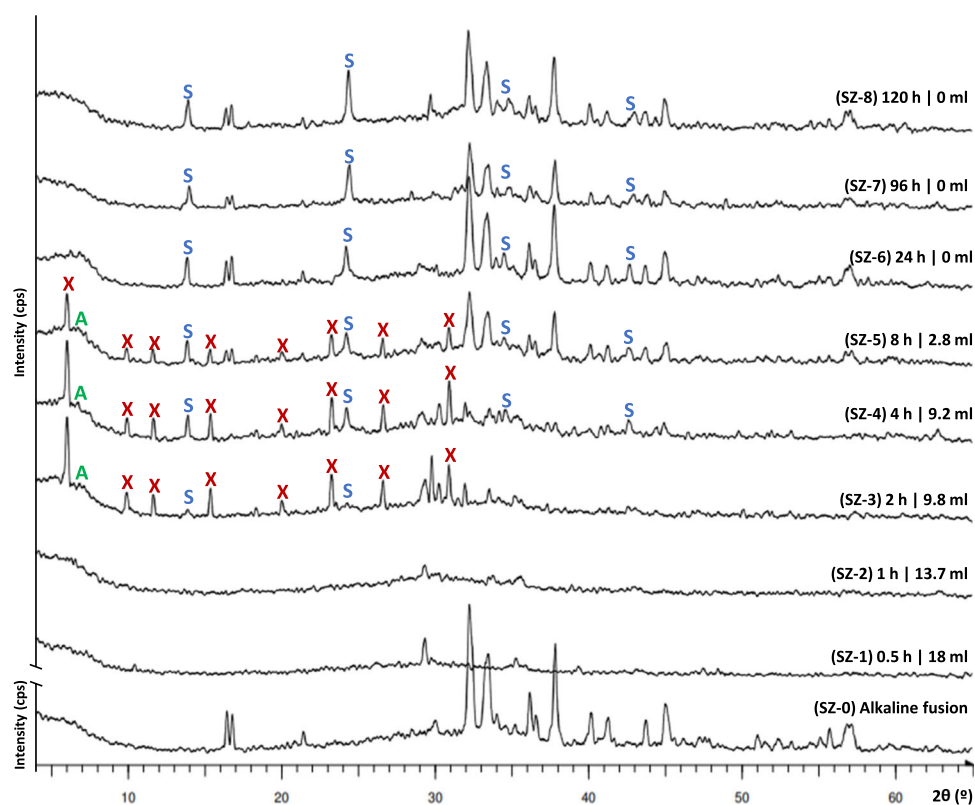


concentration of ions, mainly mixed Si^{4+} , Al^{3+} , Na^+ , and Ca^{2+} by the depolymerization in the presence of hydroxide anions (Prodinger et al. 2018). This was verified by electrical conductivity measurements taken after mixing in step 2, showing an increase from $2.63 \mu\text{S cm}^{-1}$ in the Millipore water to $>200 \text{ mS cm}^{-1}$ in the aqueous medium. At this point, the primary amorphous phase by reorganization of the chemical elements through gelation and flocculation processes, formation of three-dimensional colloidal system and its agglomeration, when generating an increasingly viscous liquid, leading to the precipitation of geopolymers creating a dense amorphous hydrogel (Cejka et al. 2011; Prodinger et al. 2018; Belviso et al. 2019). These three-dimensional polymeric structures of inorganic geopolymers are generated by chemical bonds of aluminum, silicon, and oxygen from aluminosilicate materials and alkaline solutions. Once the gel has equilibrated and transformed into a sufficiently ordered structure, secondary amorphous phase, it begins to nucleate and then polymerization begins (Prodinger et al. 2018).

In the first hour of incubation (SZ-1 and SZ-2), this amorphous aluminosilicate gel together with carbonate phases

such as calcite (PDF 47–1743, CaCO_3) and natrite (Na_2CO_3) is identified in DRX. Amorphous material together with other crystalline phases will give rise to a new nucleation and growth of different mineral phases, where dissolution, nucleation, and mineral recrystallizations coexist and in which the phases could be competitive and non-thermodynamically stable system (metastable) (Jha and Singh 2011). There was insufficient time for formation of zeolitic crystalline phases; the reaction mechanisms have not reached the zeolitic crystal growth period; it is in the induction period (Prodinger et al. 2018). After 2 h of incubation (SZ-3), a second phase of rapid growth begins, where the domains exceed one size and the peaks of the appearance of A-type hydrated zeolites (PDF 74–1185, $\text{Na}_{12}\text{Al}_{12}\text{Si}_{12}\text{O}_{48}\cdot 27\text{H}_2\text{O}$) and X-type zeolite (PDF 85–2064, $\text{NaAlSi}_{1.23}\text{O}_{4.46}\cdot 3.07\text{H}_2\text{O}$), and in smaller proportion sodalite (PDF 37–0476, $\text{Na}_4\text{Al}_3\text{Si}_3\text{O}_{12}\text{Cl}$) was observed for the first time. The continuous polymerization generates the first zeolitic precursors to give nucleation and mineral growth of zeolites entering a third period of consumption of nutrients found in the aqueous medium (Prodinger et al. 2017, 2018). Precursors can be of different nature following an unconventional crystallization, by

Fig. 5 X-ray patterns of synthesis products. The volume of aqueous solution existing at the time of completion of the synthesis process is indicated in mL. Abbreviations: A, A type zeolite (PDF 74–1183), X, X type zeolite (PDF 85–2064), S, sodalite (PDF 37–0476)



means of oligopolymers, amorphous particles, and small crystals (Oleksiak et al. 2016). During this incubation time, the crystallization climax of type X zeolite developed, as shown in Fig. 5. From this time onwards, the reduction of the hydrated zeolites in favor of sodalite occurred; mainly with a consequent increase in crystallinity to afford decomposition into a denser silica phase with a transformation (Cundy and Cox 2005).

After 8 h of incubation (SZ-5), a decrease in the intensity peaks of X-type zeolite and an increase in the intensity peaks of sodalite reflections were observed, where the complex transformation continues with the deterioration of the X-type zeolite. The volume of the aqueous medium decreased with incubation time, going from 43 mL at the initial time to 0 mL at 24 h, when the hydrothermal synthesis in the presence of a liquid phase terminates and begins the hydrothermal synthesis in the apparent absence of a liquid phase. Up to 24-h-incubation time, there is an apparent lack of a liquid phase; nevertheless, it does not mean that there is no aqueous medium; these materials contain sorbed and surface bonded water (Cundy and Cox 2005; Ivanova et al. 2017; Prodingier et al. 2017, 2018). At this time in the DRX diffractogram (Fig. 5), sodalite (thermodynamically more stable zeolite) was the predominant zeolite at longer incubation time (SZ-6, SZ-7, and SZ-8), where the specific conditions for the stabilization of sodalite have been increasing until the complete transformation

of this phase. This transformation extensively studied mainly in coal fly ash (Belviso et al. 2010, 2019; Belviso 2018) has recently also seen in the synthesis of zeolites from volcanic ash with different temperatures and water natures (Belviso et al. 2021; Gagliano et al. 2022). Sodalite, an anhydrous and thermodynamically more stable zeolite, was the predominant zeolite at longer incubation times (between 24 and 120 h).

In the case of sodalite, it is a crystalline metastable tectosilicate and competitive crystalline phase with type A and X zeolites, which have most complex inorganic transformation (Prodingier et al. 2018). When the intensity peaks of the sodalite increased, the other two zeolite intensity peaks decreased until the diffraction maxima of these two zeolites were not observed after 24 h of incubation. Sodalite was an anhydrous phase, thermodynamically more stable, and the one present at longer incubation time in this study (Walton et al. 2001; Belviso et al. 2019). At 120 h of incubation (SZ-8), no remarkable changes were observed in sodalite; however, thermonatrite and calcite increased. In this apparent absence of a liquid phase, there are no remarkable zeolitic processes in this experiment, although the synthesis of zeolite can realize in different humidity conditions (Naik et al. 2003). Therefore, the existence of the aqueous medium and time were the two principal factors that control the synthesis process of zeolites obtained from volcanic ashes following this procedure.

Synthetic products characterization

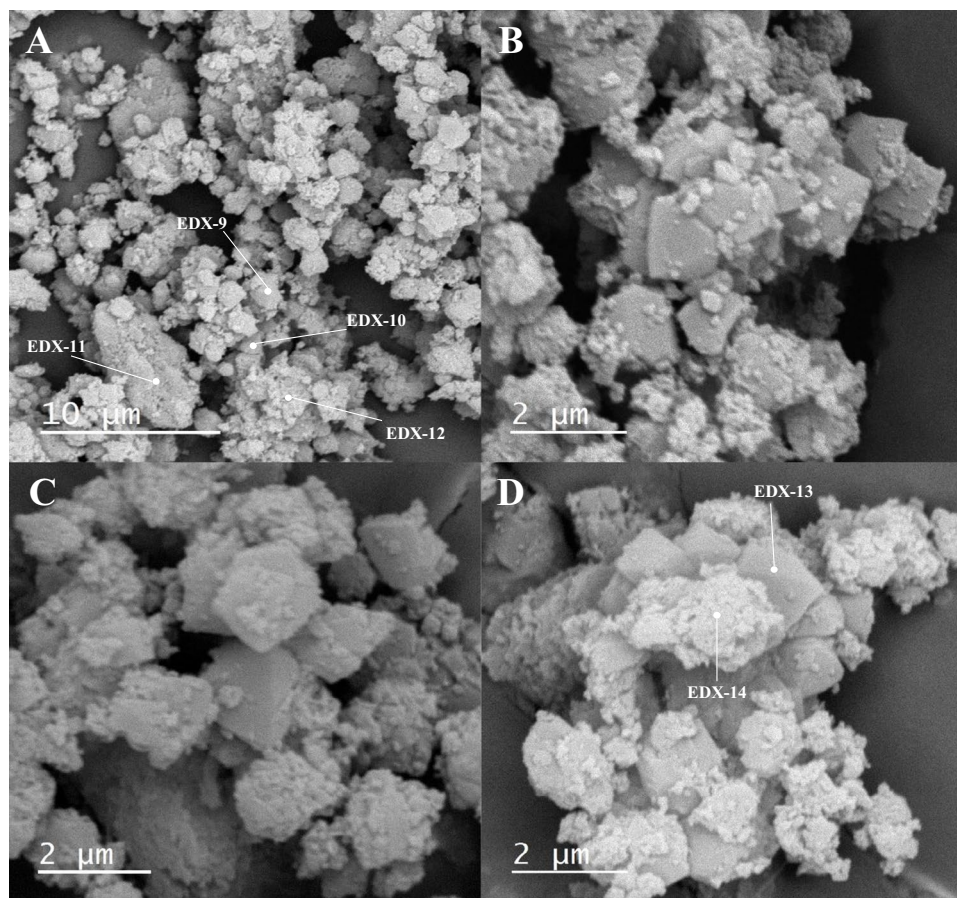
In this study, a complete analysis of sample with 2 h of incubation has been chosen for its complete characterization because it presented the first zeolites in the shortest incubation time of the process with the highest crystallinity of the X-type zeolite. The chemical analyses of major, minor, and trace elements of the synthesis product are shown in Table 2. It is worth noting the increase of Na₂O with respect to the raw material (volcanic ash, VA) from 3.5 to 12.7 wt% provided by the NaOH added in the step 1.

Morphological and textural characteristics of synthesized material analyses by SEM are shown in Fig. 6. The synthesized material was composed of heterogeneous granular aggregates in which nanometer size crystalline phases and amorphous material are found, all of them with a size of less than 10 μm. The crystalline phases of this material had 0.1 to 2 μm in size and a pseudocubic habit with smooth surfaces. Their chemical composition shown in Fig. 6 (EDX-7,

EDX-3, and EDX-4) presents the fundamental elements of the zeolite minerals. Therefore, this material can be interpreted as zeolites. XRD patterns (Fig. 5) has identified 2 types of zeolites: A and X type zeolite of Faujasite (FAU) group, and sodalite of the sodalite group, which are considered to be zeolites with low to intermediate silica/aluminium content (Jha and Singh 2011). The SiO₂/Al₂O₃ ratio of the raw material (volcanic ash in this study) was 2.74, below the limit of such ratio. It should be noted that the formula of the different zeolites identified in the PDF2 database are mainly sodic; however, the EDX analysis also presents a proportion in the calcic composition coming from the initial ash, specifically from labradorite, diopside, kaersutite, and the glassy/amorphous volcanic material.

The main crystalline phases observed in 2 h of incubation of materials by SEM can be interpreted as type X zeolite based on the XRD pattern of this sample (Fig. 5), being the most crystalline phase, since it presents the most intense peaks. In the SEM data, the presence of nanocrystal in the

Fig. 6 SEM images of the material synthesized from SZ-3 sample with 2 h of incubation: **A** Secondary electrons (SE) general image of the material at 3000×; **B**, **C**, and **D** Backscattered electrons (BSE) imagen of zeolites with aggregated material and nanocrystals on the surface at 10,000×. Spot chemical microanalysis of crystalline zeolite (EDX-9, EDX-10, and EDX-13) and amorphous and low crystalline phases (EDX-11, EDX-10, and EDX-14) (wt%)



Sample	Si	Al	Fe	Mg	Ca	Na	Ti	O
EDX-9	22.63	7.50	3.46	1.56	6.50	9.40	3.80	44.05
EDX-10	22.24	12.03	2.37	0.29	6.25	11.16	1.42	44.24
EDX-11	17.84	6.65	12.42	3.47	5.61	10.37	3.42	40.22
EDX-12	20.33	10.37	4.89	1.86	8.31	10.56	1.00	42.67
EDX-13	18.96	11.07	3.17	1.58	7.74	13.02	2.07	42.39
EDX-14	21.37	9.97	4.80	4.58	2.98	12.81	0.14	43.35

crystalline phases of the surface shows the crystalline growth process. The chemical characteristics of these nanocrystals cannot be determined due to their small size, and it was impossible to determine whether they are new X-type recrystallized zeolite or early sodalite crystals. These nanocrystals through attachment processes during mineral growth in highly saturated, gel-rich systems such as this synthesis can act as nucleation centers, facilitating zeolite growth (Ye et al. 2022). Moreover, these phases did not show crystalline alteration and reinforce the idea of climax crystallization of the X-type zeolite. It is necessary to consider that the new sodalite crystals will capture the structural element of the redissolved stock crystal and amorphous aluminosilicates. For this reason, this incubation time point is the one from which new alteration, dissolution, and recrystallization edges will be visible.

Regarding the amorphous material, it had a nanometric size with rough morphologies (Fig. 6). The chemical composition is shown in Fig. 6 (EDX-11, EDX-12, and EDX-14), being that Fe and Ti are recognized in this material, like in zeolite crystals (EDX-9, EDX-10, and EDX-13). These elements come from paramagnetic crystals (hematite, titanomagnetite, and olivine) and the abundant amorphous material of the VA. Another trace elements such as Sn, Mn, Zr, V, Cu, and Sn (Table 2) also come from VA-dissolved material incorporated in the framework structure of the synthesis material generating an increase of impurities in the zeolites (Molina and Poole 2004; Jha and Singh 2011; Zhang et al. 2022). The Fe and Ti incorporation comes from the replacement of the framework elements (Al and Si) of zeolite structures by ionic exchange or isomorphic substitution (replacement of ions without changing the overall structure of the crystal) during hydrothermal synthesis (Seddon and Zaworotko 1999; Jha and Singh 2011; Liu et al. 2019; Zhang et al. 2022; Murrieta-Rico et al. 2023). Iron can also precipitate as Fe_2O_3 on zeolite surfaces generating these amorphous materials (Belviso et al. 2021). The introduction of Fe and Ti in zeolite framework changes the physicochemical properties like the pore and redox properties, hydrophobicity, catalytic performance, and acidity, generating new applications in the chemical industry and in remediation of environmental problems of the atmospheric and water compartments (Liu et al. 2019; Zhang et al. 2022).

Preliminary study of fluoride adsorption on synthesis zeolitic materials from volcanic ash

The sources of fluorine in volcanic ash of the present study were the secondary fluorine minerals observed on the surface of the VA, originated from the interaction of gases and aerosols in the eruptive column and generating nano- and micrometric crystals on the surface of the particles during transport in the volcanic plume (Óskarsson 1980; Delmelle

et al. 2007; Ruggieri et al. 2010; Bagnato et al. 2011). An explanation for these nano and microcrystals was proposed by Óskarsson (1980) with a three temperature-zone model in which gases can interact with particles until condensation of halogenated acids at a lower temperature of 338 °C. The abundance and size of these crystals depend on the initial composition of vapors and ash particles, the duration of transport, and the surface area of the ash (the smaller the grain size, the greater the specific area, and the amount of fluorine minerals that can condense on the ash) (Óskarsson 1980; Sánchez-España et al. 2023). These minerals have a high solubility, so the deposit of ashes in the natural environment and the interaction that originates with rainwater increases fluoride concentration levels as it has been possible to analyze. This causes the mobility and dispersion of fluoride in environmental compartments (hydrosphere and biota).

Volcanoes are the main source of non-anthropogenic F^- emissions in the biosphere, causing ecological imbalance and posing a serious health risk to plants, animals, and humans in their growth and evolution (Zuo et al. 2018). Some countries with endemic fluorosis problems associated with volcanic areas are China, India, Mexico, and Ethiopia (Ayoob and Gupta 2006; Gómez-Hortigüela et al. 2013). The ingestion of fluorine-contaminated drinking water and food (vegetables and animals) leads to a loss of year of healthy life with the development of different diseases: dental and skeletal fluorosis, neurotoxic problems, renal damage, cardiovascular alterations, and endocrine dysfunction, where children and pregnant women present the highest susceptibility to develop these effects (Ayoob and Gupta 2006; Zuo et al. 2018).

The results of the VA leaching experiment show a pH of 6.37, an EC of $32.1 \mu\text{S cm}^{-1}$, and a total F concentration of 12.8 mg L^{-1} . This value exceeds the limits 8.5 times the safe drinking water limit values of fluoride in drinking waters 1.5 mg L^{-1} concentration considered dangerous to human health (World Health Organization 2022). These values with high concentrations of fluoride are observed in different studies of the hydrochemistry of the waters of La Palma from different parts of the island (Amonte et al. 2022; Rodríguez et al. 2022; Ruggieri et al. 2023; Sánchez-España et al. 2023).

One way to remediate fluoride-contaminated water is through adsorbent materials such as zeolites, as seen in different review articles (Habuda-Stanić et al. 2014; Kumar et al. 2019). It should be noted that zeolites have negatively charged surfaces at all pH levels, resulting in high adsorption of cations and low adsorption of anions due to their electrostatic repulsion when these anions approach the negatively charged surfaces (Habuda-Stanić et al. 2014). One way to adsorb fluoride is by modifying the surface of zeolite with transition cations (Sun et al. 2011). To increase the anion adsorption capacity with zeolites, there are different authors

who have used natural zeolites rich in sodium and calcium (Gómez-Hortigüela et al. 2013), surface modifications of modified natural stibite zeolites with Fe^{3+} (Sun et al. 2011; Ranasinghe et al. 2022), with Al^{3+} (Teutli-Sequeira et al. 2014), calcium chloride (CaCl_2)-modified natural zeolite (Zhang et al. 2011), modified with Al^{3+} and Fe^{3+} (Rahmani et al. 2010), F-9 zeolite modified with Al^{3+} and La^{3+} (Onyango et al. 2004).

The results obtained from the batch adsorption test with alkaline pH has evidence that the best adsorption result of the 0.5 g L^{-1} dose was found in the SZ-6 (24-h-synthesis incubation) sample with 28.9% of efficiency adsorption and 3.7 mg L^{-1} F total removal followed by the SZ-4 (4 h synthesis incubation) with 25.8 E% and SZ-3 (2 h synthesis incubation) sample with 20.3% efficiency removal and 2.6 mg L^{-1} F total removal. At the dose of 2 g L^{-1} , higher efficiency adsorption was found in sample SZ-4 (4 h synthesis incubation) sample with 22.7% efficiency removal and 2.9 mg L^{-1} F total reduction, followed by SZ-6 (24 synthesis incubation) sample with 19.5% efficiency removal and 2.5 mg L^{-1} F total reduction and then, SZ-3 (2 h synthesis incubation) sample with 17.9% efficiency removal and 2.3 mg L^{-1} F total reduction. We have performed another experiment to see what changes occur at acidic pH in 2 h of contact time of adsorbent material with volcanic leachate medium. In this experiment with acidic pH (5.74 to 5.77), the best result obtained from SZ-4 sample (4-h-synthesis incubation) was from 2 g L^{-1} doses with 41.4% adsorption efficiency with 5.3 mg L^{-1} F total reduction, followed by 0.5 g L^{-1} doses with 22.7% removal efficiency and 2.9 mg L^{-1} F total reduction. The decrease in time in the new experiment need not have a significant effect, as there are multitude of articles pointing to rapid activity in the adsorption of aqueous fluoride on zeolites, as noted by Xu et al. (2011) and Waghmare et al. (2015), the adsorption rate of the product was 1 h. Panda and Kar (2018) point out that, in 30 min, they obtain equilibrium, and Lü et al. 2010 comment that it is a fast process, and they observe how in 20 min the adsorption stabilize with an elimination rate of 92.97%. Therefore, this increase in efficiency comes from the effect of acidic pH; authors such as Chen et al. (2022) point out that the optimum pH is at 5.5–6.5 for zeolite loaded with aluminum hydroxide; Panda and Kar (2018) point out that the optimum adsorption efficiency is around pH 6 for NAP1 type zeolite. Ranasinghe et al. (2022) state that the maximum fluoride removal of 92% is below pH 3 in Fe^{3+} -modified zeolite. Apart from these parameters, the initial concentration of fluoride in the water and the dosage of adsorbent material and fluoride aqua should be checked, since the % removal of the 0.5 g L^{-1} dosage at acid pH shows a lower removal efficiency than in the same sample with alkaline pH aqueous medium.

Therefore, in the present work, data on remediation of water contaminated by F of volcanic origin are presented

for the first-time using zeolites synthesized from a residue of the same volcanic activity that causes the problem. The efficiency data can be considered preliminary, but very promising, with rates that reach values of 41.4% of the fluorine present in the leachates. This preliminary adsorption data allows the End Waste principle with the recycling of waste and obtaining a beneficial material for the environment and human health, according to the principles of Circular Economy and promoting United Nations Sustainable Development Goals of 2030 Agenda (SDG 3—“Good Health and Well-Being”, 6—“Clean Water and Sanitation” and 12—“Responsible Consumption and Production”) (Naciones Unidas/CEPAL 2019) with defluoridation of La Palma’s contaminated water. A material to adsorb fluoride is obtained cheaply and with a locally accessible raw material (volcanic ash).

Conclusions

In this study, different types of zeolites were synthesized from volcanic ashes from the Tajogaite 2021 event in La Palma with a hydrothermal treatment at $100 \text{ }^\circ\text{C}$ with previous melting at $550 \text{ }^\circ\text{C}$.

The characterization of the VA has shown crystalline phases (kaersutite, plagioclase, olivine, pyroxene, titanomagnetite, ilmenite, and hematite) with a high content of amorphous material observed in XRD and SEM. The chemical composition of this material was mainly aluminosilicate, with high amounts of Fe_2O_3 (15.05 wt%), CaO (12.03%), and TiO_2 (4.26 wt%) as oxides. Secondary minerals with high fluorine content (from 43.98 to 51.41 wt%), interpreted as soluble AlF_3 and CaF_2 minerals, are observed on the surface of all particles.

Following the pre-melting hydrothermal synthesis methodology used in this study, the three zeolites, type A, type X, and sodalite, are identified at 2 h of incubation. At this time, the crystallographic climax of type X zeolite is observed, with no dissolution features in SEM. In the following 6 h, processes of metastability and competitiveness between type X zeolites and sodalite are observed, where the former decreases with respect to the latter, through a continuous transformation to a thermodynamically more stable zeolite. After 24 h, when the aqueous medium evaporates, sodalite begins to predominate.

The synthesized materials presented zeolites with high crystallinity coated by amorphous and less crystalline phases. Regarding the chemical characteristics of these materials, it is worth mentioning the presence of Ti and Fe both in the zeolites, incorporated as impurities during the synthesis process, and in the amorphous material, coming from the raw minerals, titanomagnetite, ilmenite, and hematite, mainly. As for the increase of sodium in

the synthesized material, it comes from the NaOH introduced in the first stage of the synthesis methodology, generating a zeolite with high concentration of Na₂O (12.70 wt%) and CaO (11.65 wt%) and as exchange cations and Fe₂O₃ (13.70%) and TiO₂ (3.89 wt%) as impurities introduced by isomorphic substitution, which can modify the physicochemical properties generating a material that can solve a local problem such as fluoride contamination in the environment.

The F adsorption tests on the produced zeolites have shown high adsorption efficiencies of up to 41.4% at acidic pH, and lower efficiencies (18.0–28.9%) at alkaline pH in the preliminary experiments. The efficiencies at basic pH have been similar in all types of zeolites, both type X climax (SZ-3), type X + sodalite (SZ-4), and sodalite (SZ-6). To our knowledge, for the first time, it has been possible to propose a solution to an environmental problem generated by volcanic activity from a waste produced in the same eruptive process. With the application of this method to volcanic ashes, classified as municipal waste, it has been possible to demonstrate the ability to form zeolites giving an added value to the material, promoting the circular economy, allowing fully recovering of waste following the “End of Waste” criteria proposed by Waste framework directive 2008/98/EC (European Council 2008) and resulting in meeting different SDG goals of the UN Agenda 2030.

Future research on zeolite synthesis from volcanic ash should focus on studying different times and temperatures to match the research that has been done to date with fly ash. Likewise, it is convenient to explore the different capacities provided by the impurities of Fe, Ca, Na, and Ti in the zeolitic material and the adsorption of fluorides in the zeolites at different pHs and doses until finding the optimal conditions for maximum adsorption defluorination efficiency.

Acknowledgements We are grateful to the Department of Mineralogy and Petrology for the use of the laboratory and to the Unidad de Técnicas Geológicas (CAI de Ciencias de la Tierra y Arqueometría, UCM), especially to Xabier Arroyo-Rey for his advice in the management of analytical equipment.

Author contribution The conception of the study was performed by Iker Martínez-del-Pozo, Luz García-Lorenzo, and Sol López-Andrés. Material preparation, data collection, and analysis were performed by Iker Martínez-del-Pozo and Sol López-Andrés. The first draft of the manuscript was written by Iker Martínez-del-Pozo. The manuscript was reviewed and edited by Iker Martínez-del-Pozo, José María Esbrí, Luz García-Lorenzo, and Sol López-Andrés, and all the authors commented on the previous versions of the manuscript. All the authors read and approved the final manuscript.

Funding This research was funded by 910386 UCM Investigation Group “Técnicas cristalográficas y geológicas. Aplicaciones no convencionales”, with the help of Spanish “Ministerio de Ciencia e Innovación” Project (TED2021-130498B-I00) and the Spanish “Ministerio de Trabajo y Economía Social” (INVESTIGO program CT19/23-INVM-120).

Data Availability The data that support the findings of this study are available from the corresponding author, [antares@ucm.es], upon reasonable request.

Declarations

Ethics approval Not applicable.

Consent to participate Not applicable.

Consent for publication Not applicable.

Competing interests The authors declare no competing interests.

References

- Almirón J, Vargas M, Tupayachy-Quispe D et al (2022) Influence of the process of synthesis of zeolites from volcanic ash in its synergistic action as a flame-retardant for polypropylene composites. *Buildings* 12:24. <https://doi.org/10.3390/buildings12010024>
- Amonte C, Melián GV, Asensio-Ramos M et al (2022) Hydrogeochemical temporal variations related to the recent volcanic eruption at the Cumbre Vieja Volcano, La Palma, Canary Islands. *Front Earth Sci (lausanne)* 10:1003890. <https://doi.org/10.3389/feart.2022.1003890>
- Arroyo X, Andreu L, López-Andrés S, García-Lorenzo ML (2021) Caracterización de materiales geológicos del volcán de Cumbre Vieja (La Palma, España) y su posible revalorización como materia prima en aplicaciones ambientales. In: García Romero E, Fernández Barrenechea J, García Rivas J, Arroyo Rey X, del Buey Fernández P (ed) Libro de resúmenes de la XXVII Reunión de la Sociedad Española de Arcillas. Sociedad Española de Arcillas, Madrid, España, pp 13–14
- Ayoob S, Gupta AK (2006) Fluoride in drinking water: a review on the status and stress effects. *Crit Rev Environ Sci Technol* 36:433–487. <https://doi.org/10.1080/10643380600678112>
- Bagnato E, Aiuppa A, Andronico D, et al (2011) Leachate analyses of volcanic ashes from Stromboli volcano: a proxy for the volcanic gas plume composition?. *J Geophys Res Atmos* 116. <https://doi.org/10.1029/2010JD015512>
- Barone G, Mazzoleni P, Corsaro RA et al (2016) Nanoscale surface modification of Mt. Etna volcanic ashes. *Geochim Cosmochim Acta* 174:70–84. <https://doi.org/10.1016/j.gca.2015.11.011>
- Barsotti S, Andronico D, Neri A et al (2010) Quantitative assessment of volcanic ash hazards for health and infrastructure at Mt. Etna (Italy) by numerical simulation. *J Volcanol Geoth Res* 192:85–96. <https://doi.org/10.1016/j.jvolgeores.2010.02.011>
- Belviso C (2018) Ultrasonic vs hydrothermal method: different approaches to convert fly ash into zeolite. How they affect the stability of synthetic products over time? *Ultrason Sonochem* 43:9–14. <https://doi.org/10.1016/j.ultsonch.2017.12.050>
- Belviso C, Cavalcante F, Fiore S (2010) Synthesis of zeolite from Italian coal fly ash: differences in crystallization temperature using seawater instead of distilled water. *Waste Manag* 30:839–847. <https://doi.org/10.1016/j.wasman.2009.11.015>
- Belviso C, Cavalcante F, Javier Huertas F et al (2012) The crystallisation of zeolite (X- and A-type) from fly ash at 25 °C in artificial sea water. *Microporous Mesoporous Mater* 162:115–121. <https://doi.org/10.1016/j.micromeso.2012.06.028>
- Belviso C, Perchiazzi N, Cavalcante F (2019) Zeolite from fly ash: an investigation on metastable behavior of the newly formed minerals in a medium-high-temperature range. *Ind Eng Chem Res* 58(44):20472–20480. <https://doi.org/10.1021/acs.iecr.9b03784>

- Belviso C, Abdolrahimi M, Peddis D et al (2021) Synthesis of zeolite from volcanic ash: characterization and application for cesium removal. *Microporous Mesoporous Mater* 319:111045. <https://doi.org/10.1016/j.micromeso.2021.111045>
- Blanton TN, Huang TC, Toraya H, Hubbard CR, Robie SB, Louër D, Göbel HE, Gilles R, Raftery T (1995) JCPDS-International centre for diffraction data round robin study of silver behenate. A possible low-angle X-ray diffraction calibration standard. *Powder Diffr* 10(2):91–95. <https://doi.org/10.1017/S0885715600014421>
- Bonadonna C, Pistolesi M, Biass S et al (2022) Physical characterization of long-lasting hybrid eruptions: the 2021 Tajogaite eruption of Cumbre Vieja (La Palma, Canary Islands). *J Geophys Res Solid Earth* 127:e2022JB025302. <https://doi.org/10.1029/2022JB025302>
- Carracedo JC, Troll VR, Day JMD et al (2022) The 2021 eruption of the Cumbre Vieja volcanic ridge on La Palma, Canary Islands. *Geol Today* 38:94–107. <https://doi.org/10.1111/gto.12388>
- Cejka J, Corma A, Zones S (2011) Zeolites and catalysis. Synthesis, reactions and applications. WILEY-VCH Verlag GmbH & Co. KGaA, Weinheim
- Chang HL, Shih WH (1998) A general method for the conversion of fly ash into zeolites as ion exchangers for cesium. *Ind Eng Chem Res* 37:71–78. <https://doi.org/10.1021/ie970362o>
- Chen J, Yang R, Zhang Z, Wu D (2022) Removal of fluoride from water using aluminum hydroxide-loaded zeolite synthesized from coal fly ash. *J Hazard Mater* 421:126817. <https://doi.org/10.1016/j.jhazmat.2021.126817>
- Cundy CS, Cox PA (2005) The hydrothermal synthesis of zeolites: precursors, intermediates and reaction mechanism. *Microporous Mesoporous Mater* 82:1–78
- Delmelle P, Lambert M, Dufrière Y et al (2007) Gas/aerosol-ash interaction in volcanic plumes: new insights from surface analyses of fine ash particles. *Earth Planet Sci Lett* 259:159–170. <https://doi.org/10.1016/j.epsl.2007.04.052>
- Environmental Protection Agency (2010) Guidance on classification of waste according to EWC-Stat categories. Eurostat. <https://ec.europa.eu/eurostat/documents/342366/351806/Guidance-on-EWCStat-categories-2010.pdf/0e7cd3fc-c05c-47a7-818f-1c2421e55604>. Accessed 22 Dec 2023
- Ermolin MS, Fedotov PS, Malik NA, Karandashev VK (2018) Nanoparticles of volcanic ash as a carrier for toxic elements on the global scale. *Chemosphere* 200:16–22. <https://doi.org/10.1016/j.chemosphere.2018.02.089>
- European Council (2008) Directive 2008/98/EC of the European Parliament and of the Council of 19 November 2008 on waste and repealing certain Directives. Official Journal of the European Union. <http://data.europa.eu/eli/dir/2008/98/oj>. Accessed 22 Dec 2023
- Fernández-Turiel JL, Saavedra-Alonso J, Ruggieri F, et al (2012) Geochemistry of volcanic ash along two transects in South America: environmental implications. *Geo-Temas* 1–32
- Gagliano E, Sgroi M, Falciglia PP et al (2022) Removal of ammonium from wastewater by zeolite synthesized from volcanic ash: batch and column tests. *J Environ Chem Eng* 10:107539. <https://doi.org/10.1016/j.jece.2022.107539>
- Ge Q, Moeen M, Tian Q et al (2020) Highly effective removal of Pb²⁺ in aqueous solution by Na-X zeolite derived from coal gangue. *Environ Sci Pollut Res* 27:7398–7408. <https://doi.org/10.1007/s11356-019-07412-z>
- Gómez-Hortigüela L, Pérez-Pariente J, García R et al (2013) Natural zeolites from Ethiopia for elimination of fluoride from drinking water. *Sep Purif Technol* 120:224–229. <https://doi.org/10.1016/j.seppur.2013.10.006>
- Habuda-Stanić M, Ravančić M, Flanagan A (2014) A review on adsorption of fluoride from aqueous solution. *Materials* 7:6317–6366. <https://doi.org/10.3390/ma7096317>
- Hamoud MA, Abo-Zahra SF, Attia MA et al (2023) Efficient adsorption of cesium cations and chromate anions by one-step process using surfactant-modified zeolite. *Environ Sci Pollut Res* 30:53140–53156. <https://doi.org/10.1007/s11356-023-25644-y>
- Han C, Yang T, Liu H et al (2019) Characterizations and mechanisms for synthesis of chitosan-coated Na-X zeolite from fly ash and As(V) adsorption study. *Environ Sci Pollut Res* 26:10106–10116. <https://doi.org/10.1007/s11356-019-04466-x>
- He K, Chen Y, Tang Z, Hu Y (2016) Removal of heavy metal ions from aqueous solution by zeolite synthesized from fly ash. *Environ Sci Pollut Res* 23:2778–2788. <https://doi.org/10.1007/s11356-015-5422-6>
- Horwell CJ, Baxter PJ (2006) The respiratory health hazards of volcanic ash: a review for volcanic risk mitigation. *Bull Volcanol* 69:1–24. <https://doi.org/10.1007/s00445-006-0052-y>
- Ivanova II, Kolyagin YG, Kasyanov IA et al (2017) Time-resolved in situ MAS NMR monitoring of the nucleation and growth of zeolite BEA catalysts under hydrothermal conditions. *Angew Chemie – Int Ed* 56:15344–15347. <https://doi.org/10.1002/anie.201709039>
- Jenkins SF, Wilson T, Magill C, Stewart C, Blong R, Marzocchi W, Boulton M, Bonadonna C, Costa A (2015). Volcanic ash fall hazard and risk. In: Loughlin SC, Sparks S, Brown SK, Jenkins SF, Vye-Brown C (ed) *Global Volcanic Hazards and Risk*, Cambridge University Press, pp 173–222
- Jha B, Singh DN (2011) A review on synthesis, characterization and industrial applications of fly ash zeolites. *J Mater Educ* 33:65–132. <https://doi.org/10.1002/chin.201225227>
- Jones MT, Gislason SR (2008) Rapid releases of metal salts and nutrients following the deposition of volcanic ash into aqueous environments. *Geochim Cosmochim Acta* 72:3661–3680. <https://doi.org/10.1016/j.gca.2008.05.030>
- Kumar PS, Suganya S, Srinivas S et al (2019) Treatment of fluoride-contaminated water. A review. *Environ Chem Lett* 17:1707–1726. <https://doi.org/10.1007/s10311-019-00906-9>
- Kupwade-Patil K, Chin SH, Johnston ML et al (2018) Particle size effect of volcanic ash towards developing engineered Portland cements. *J Mater Civ Eng* 30:04018190. [https://doi.org/10.1061/\(asce\)mt.1943-5533.0002348](https://doi.org/10.1061/(asce)mt.1943-5533.0002348)
- Le Maitre RW, Streckeisen A, Zanettin B, Le Bas MJ, Bonin B, Bate-man P (2005) *Igneous rocks: a classification and glossary of terms: recommendations of the International Union of Geological Sciences Subcommittee on the Systematics of Igneous Rocks*. Cambridge University Press, Cambridge
- Lechner P, Tupper A, Guffanti M et al (2018) Volcanic ash and aviation—the challenges of real-time, global communication of a natural hazard. In: Fearnley Carina J, Bird Deanne K, Katherine H et al (eds) *Advances in volcanology*. Springer, Cham, Barcelona, Spain, pp 51–64
- Lee MG, Park JW, Kam SK, Lee CH (2018) Synthesis of Na-A zeolite from Jeju Island scoria using fusion/hydrothermal method. *Chemosphere* 207:203–208. <https://doi.org/10.1016/j.chemosphere.2018.05.080>
- Liu H, Yue Y, Shen T et al (2019) Transformation and crystallization behaviors of titanium species in synthesizing Ti-ZSM-5 zeolites from natural rectorite mineral. *Ind Eng Chem Res* 58:11861–11870. <https://doi.org/10.1021/acs.iecr.9b01826>
- Longpré MA, Felpeto A (2021) Historical volcanism in the Canary Islands; part 1: a review of precursory and eruptive activity, eruption parameter estimates, and implications for hazard assessment. *J Volcanol Geoth Res* 419:107363. <https://doi.org/10.1016/j.jvolgeores.2021.107363>
- López-Delgado A, Padilla I, Sánchez-Hernández R, Rodríguez O, López-Andrés S (2017) Procedimiento de revalorización de un residuo procedente de la molienda de escorias de aluminio. <http://hdl.handle.net/10261/176220>. Accessed 22 Dec 2023

- López-Delgado A, Robla JI, Padilla I et al (2020) Zero-waste process for the transformation of a hazardous aluminum waste into a raw material to obtain zeolites. *J Clean Prod* 255:120178. <https://doi.org/10.1016/j.jclepro.2020.120178>
- Lü H, Wang B, Ban Q (2010) Defluoridation of drinking water by zeolite NaP1 synthesized from coal fly ash. *Energy Sources, Part A: Recovery, Util Environ Eff* 32:1509–1516. <https://doi.org/10.1080/15567030902780352>
- Luévano-Hipólito E, Torres-Martínez LM, Fernández-Trujillo A (2021) Ternary ZnO/CuO/Zeolite composite obtained from volcanic ash for photocatalytic CO₂ reduction and H₂O decomposition. *J Phys Chem Solids* 151:109917. <https://doi.org/10.1016/j.jpms.2020.109917>
- Mañosa J, Serrano-Conte J, Maldonado-Alameda A et al (2023) Pyroclastic volcanic ash as a potential precursor of alkali-activated binders – a case study from Tajogaite (La Palma, Canary Islands) volcano eruption. *J Build Eng* 72:106623. <https://doi.org/10.1016/j.job.2023.106623>
- Martin JD (2004) Using X Powder: a software package for powder x-ray diffraction analysis. 84-609-1497-6, D.L. GR 1001/04. <http://www.xpowder.com>. Accessed 22 Dec 2023
- Molina A, Poole C (2004) A comparative study using two methods to produce zeolites from fly ash. *Miner Eng* 17:167–173. <https://doi.org/10.1016/j.mineng.2003.10.025>
- Monzón JD, Gonzalez MR, Muñoz M et al (2021) Phase-transition process in the hydrothermal zeolitization of volcanic ash into LTA and FAU structures. *Clays Clay Miner* 69:735–745. <https://doi.org/10.1007/s42860-021-00148-3>
- Muñoz M, Pasquale G, Sathicq AG et al (2019) Volcanic ash as reusable catalyst in the green synthesis of 3H–1,5-benzodiazepines. *Green Process Synth* 8:600–610. <https://doi.org/10.1515/gps-2019-0030>
- Muñoz M, Pereyra AM, Gonzalez MR et al (2023) Zeolitized volcanic ashes as supports for Anderson heteropolycompound catalysts. Application in the oxidation of diphenyl sulfide. *Mater Today Commun* 34:105459. <https://doi.org/10.1016/j.mtcomm.2023.105459>
- Muñoz Pérez Sócrates P, Charca Mamani S, Dávila Gamonal CM et al (2022) Use of fly ash in the production of geopolymers: a literature review. *Innov Infrastruct Solut* 7:236. <https://doi.org/10.1007/s41062-022-00835-7>
- Murrieta-Rico FN, Antúnez-García J, Yocupicio-Gaxiola RI et al (2023) One-pot synthesis of iron-modified zeolite X and characterization of the obtained materials. *Catalysts* 13:1159. <https://doi.org/10.3390/catal13081159>
- Naciones Unidas/CEPAL (2019) La Agenda 2030 y los Objetivos de Desarrollo Sostenible: una oportunidad para América Latina y el Caribe. Objetivos, metas e indicadores mundiales. <https://hdl.handle.net/11362/40155>. Accessed 22 Dec 2023
- Naik SP, Chiang AST, Thompson RW (2003) Synthesis of zeolitic mesoporous materials by dry gel conversion under controlled humidity. *J Phys Chem B* 107:7006–7014. <https://doi.org/10.1021/jp034425u>
- Novembre D, Di Sabatino B, Gimeno D et al (2004) Synthesis of Na-X zeolites from tripolaceous deposits (Crotone, Italy) and volcanic zeolitised rocks (Vico volcano, Italy). *Microporous Mesoporous Mater* 75:1–11. <https://doi.org/10.1016/j.micromeso.2004.06.022>
- Oleksiak MD, Soltis JA, Conato MT et al (2016) Nucleation of FAU and LTA zeolites from heterogeneous aluminosilicate precursors. *Chem Mater* 28:4906–4916. <https://doi.org/10.1021/acs.chemmater.6b01000>
- Onyango MS, Kojima Y, Aoyi O et al (2004) Adsorption equilibrium modeling and solution chemistry dependence of fluoride removal from water by trivalent-cation-exchanged zeolite F-9. *J Colloid Interface Sci* 279:341–350. <https://doi.org/10.1016/j.jcis.2004.06.038>
- Óskarsson N (1980) The interaction between volcanic gases and tephra: fluoride adhering to tephra of the 1970 hekla eruption. *J Volcanol Geoth Res* 8:251–266. [https://doi.org/10.1016/0377-0273\(80\)90107-9](https://doi.org/10.1016/0377-0273(80)90107-9)
- Otieno SO, Kengara FO, Kowenje CO, Mokaya R (2023) Hydrothermal synthesis of zeolites using silica extracted from tropical volcanic ash. *Mater Adv* 4:2292–2300. <https://doi.org/10.1039/d3ma00065f>
- Panda L, Kar BB (2018) Preparation of fly ash based zeolite for fluoride removal. *Asian J Water Environ Pollut* 15:105–113. <https://doi.org/10.3233/AJW-180063>
- Prodinger S, Shi H, Eckstein S et al (2017) Stability of zeolites in aqueous phase reactions. *Chem Mater* 29:7255–7262. <https://doi.org/10.1021/acs.chemmater.7b01847>
- Prodinger S, Vjunov A, Hu JZ et al (2018) Elementary steps of faujasite formation followed by in situ spectroscopy. *Chem Mater* 30:888–897. <https://doi.org/10.1021/acs.chemmater.7b04554>
- Rahmani A, Nouri J, Kamal Ghadiri S et al (2010) Adsorption of fluoride from water by Al³⁺ and Fe³⁺ pretreated natural Iranian zeolites. *Int J Environ Res* 4:607–614
- Ranasinghe RAJC, Hansima MACK, Nanayakkara KGN (2022) Adsorptive removal of fluoride from water by chemically modified coal fly ash: synthesis, characterization, kinetics, and mechanisms. *Groundw Sustain Dev* 16:100699. <https://doi.org/10.1016/j.gsd.2021.100699>
- Rodríguez F, Pérez NM, Amonte C, Martín-Lorenzo A, Melián GV, Coldwell BC, Pankhurst MJ, Asensio-Ramos M, Hernández PA, Padrón E (2022) Geochemistry of ash leachates during the 2021 eruption of Cumbre Vieja volcano, La Palma, Canary Islands. *Display*. <https://doi.org/10.5194/egusphere-egu22-9629>
- Ruano-Ravina A, Acosta O, Díaz Pérez D et al (2023) A longitudinal and multidesign epidemiological study to analyze the effect of the volcanic eruption of Tajogaite volcano (La Palma, Canary Islands). The ASHES study protocol. *Environ Res* 216:114486. <https://doi.org/10.1016/j.envres.2022.114486>
- Ruggieri F, Saavedra J, Fernandez-Turiel JL et al (2010) Environmental geochemistry of ancient volcanic ashes. *J Hazard Mater* 183:353–365. <https://doi.org/10.1016/j.jhazmat.2010.07.032>
- Ruggieri F, Gil RA, Fernandez-Turiel JL et al (2012) Multivariate factorial analysis to design a robust batch leaching test to assess the volcanic ash geochemical hazard. *J Hazard Mater* 213:273–284. <https://doi.org/10.1016/j.jhazmat.2012.01.091>
- Ruggieri F, Forte G, Bocca B et al (2023) Potentially harmful elements released by volcanic ash of the 2021 Tajogaite eruption (Cumbre Vieja volcano, Canary Island, Spain): implications for human health. *Sci Total Environ* 905:167103. <https://doi.org/10.1016/j.scitotenv.2023.167103>
- Sánchez-España J, Mata MP, Vegas J et al (2023) Leaching tests reveal fast aluminum fluoride release from ashfall accumulated in La Palma (Canary Islands, Spain) after the 2021 Tajogaite eruption. *J Volcanol Geoth Res* 444:107959. <https://doi.org/10.1016/j.jvolgeores.2023.107959>
- Sánchez-Hernández R, López-Delgado A, Padilla I et al (2016) One-step synthesis of NaP1, SOD and ANA from a hazardous aluminum solid waste. *Microporous Mesoporous Mater* 226:267–277. <https://doi.org/10.1016/j.micromeso.2016.01.037>
- Sánchez-Hernández R, Padilla I, López-Andrés S, López-Delgado A (2017) Eco-friendly bench-scale zeolitization of an Al-containing waste into gismondine-type zeolite under effluent recycling. *J Clean Prod* 161:792–802. <https://doi.org/10.1016/j.jclepro.2017.05.201>
- Sánchez-Hernández R, Padilla I, López-Andrés S, López-Delgado A (2018a) Single and competitive adsorptive removal of lead, cadmium, and mercury using zeolite adsorbent prepared from industrial aluminum waste. *Desalin Water Treat* 126:181–195. <https://doi.org/10.5004/dwt.2018.22816>

- Sánchez-Hernández R, Padilla I, López-Andrés S, López-Delgado A (2018b) Al-waste-based zeolite adsorbent used for the removal of ammonium from aqueous solutions. *Int J Chem Eng* 2018:11. <https://doi.org/10.1155/2018/1256197>
- Sanhueza-Núñez VM, Bennun-Torres LD (2015) Synthesis of zeolitic materials from volcanic ash in presence and absence of cetyltrimethylammonium bromide. *Revista Internacional De Contaminacion Ambiental* 31:185–193
- Seddon KR, Zaworotko M (1999) *Crystal engineering: the design and application of functional solids*, 1st edn. Springer Science & Business Media, Digby, Nova Scotia, Canada
- Stewart C, Damby DE, Tomašek I, Horwell CJ, Plumlee GS, Armienta MA, Hinojosa MGR, Appleby M, Delmelle P, Cronin S, Ottley CJ, Oppenheimer C, Morman S (2020) Assessment of leachable elements in volcanic ashfall: a review and evaluation of a standardized protocol for ash hazard characterization. *J Volcanol Geotherm Res* 392:106756. <https://doi.org/10.1016/j.jvolgeores.2019.106756>
- Sun Y, Fang Q, Dong J et al (2011) Removal of fluoride from drinking water by natural stilbite zeolite modified with Fe(III). *Desalination* 277:121–127. <https://doi.org/10.1016/j.desal.2011.04.013>
- Teutli-Sequeira A, Solache-Ríos M, Martínez-Miranda V, Linares-Hernández I (2014) Comparison of aluminum modified natural materials in the removal of fluoride ions. *J Colloid Interface Sci* 418:254–260. <https://doi.org/10.1016/j.jcis.2013.12.020>
- Waghmare S, Arfin T, Rayalu S et al (2015) Adsorption behavior of modified zeolite as novel adsorbents for fluoride removal from drinking water: surface phenomena, kinetics and thermodynamics studies. *Int J Sci Eng Technol Res* 4:4114–4124. <https://doi.org/10.5194/egusphere-egu22-9629>
- Walton RI, Millange F, O'Hare D et al (2001) In situ energy-dispersive X-ray diffraction study of the hydrothermal crystallization of zeolite A. 1. Influence of reaction conditions and transformation into sodalite. *J Phys Chem B* 105:83–90. <https://doi.org/10.1021/jp002711p>
- Wang Y, Luo M, Xu F, Zhang W (2015) Conversion of volcanic tephra to zeolites for calcium ion cross-linked alginate-zeolite composites for enhanced aqueous removal of Cu(II) ions. *Water Air Soil Pollut* 226:1–13. <https://doi.org/10.1007/s11270-015-2554-8>
- Wen J, Yan C, Xing L et al (2021) Simultaneous immobilization of As and Cd in a mining site soil using HDTMA-modified zeolite. *Environ Sci Pollut Res* 28:9935–9945. <https://doi.org/10.1007/s11356-020-11477-6>
- WHO (2022) *Guidelines for drinking-water quality fourth edition incorporating the first and second addenda* WHO Press. World Health Organization, Geneva, Switzerland. <http://www.who.int/publications/i/item/9789240045064>. Accessed 22 Dec 2023
- Xu X, Li Q, Cui H et al (2011) Adsorption of fluoride from aqueous solution on magnesia-loaded fly ash cenospheres. *Desalination* 272:233–239. <https://doi.org/10.1016/j.desal.2011.01.028>
- Ye Z, Zhao Y, Zhang H et al (2022) Mesocrystal morphology regulation by “alkali metals ion switch”: re-examining zeolite nonclassical crystallization in seed-induced process. *J Colloid Interface Sci* 608:1366–1376. <https://doi.org/10.1016/j.jcis.2021.10.125>
- Zhang Z, Tan Y, Zhong M (2011) Defluorination of wastewater by calcium chloride modified natural zeolite. *Desalination* 276:246–252. <https://doi.org/10.1016/j.desal.2011.03.057>
- Zhang J, Tang X, Yi H et al (2022) Synthesis, characterization and application of Fe-zeolite: a review. *Appl Catal A Gen* 630:118467. <https://doi.org/10.1016/j.apcata.2021.118467>
- Zhou X, Shi S, Ding B, et al (2023) Optimization of preparation of NaA zeolite from fly ash for CO₂ capture. *Environ Sci Pollut Res* 1–15. <https://doi.org/10.1007/s11356-023-29648-6>
- Zuo H, Chen L, Kong M et al (2018) Toxic effects of fluoride on organisms. *Life Sci* 198:18–24. <https://doi.org/10.1016/j.lfs.2018.02.001>

Publisher's Note Springer Nature remains neutral with regard to jurisdictional claims in published maps and institutional affiliations.

Springer Nature or its licensor (e.g. a society or other partner) holds exclusive rights to this article under a publishing agreement with the author(s) or other rightsholder(s); author self-archiving of the accepted manuscript version of this article is solely governed by the terms of such publishing agreement and applicable law.